



Decolorization of Rhodamine B by silver nanoparticle–loaded magnetic sporopollenin: characterization and process optimization

Ümit Ecer¹ · Tekin Şahan² · Adem Zengin² · İlkey Hilal Gubbuk³

Received: 31 January 2022 / Accepted: 7 June 2022 / Published online: 16 June 2022
© The Author(s), under exclusive licence to Springer-Verlag GmbH Germany, part of Springer Nature 2022

Abstract

Silver nanoparticles (Ag NPs) were reduced on the surface of magnetic sporopollenin (Fe₃O₄@SP) modified with polydopamine to enhance the degradation capability for Rhodamine B (RhB). The polydopamine-coated Fe₃O₄@SP (PDA@Fe₃O₄@SP) acts as a self-reducing agent for Ag⁺ ions to Ag⁰. The structural properties of the synthesized nanocomposite were determined using Fourier transform infrared spectrometry (FTIR), scanning electron microscopy (SEM), X-ray photoelectron spectroscopy (XPS), X-ray powder diffraction (XRD), inductively coupled plasma mass spectrometry (ICP-MS), and vibrating sample magnetometer (VSM). The systematic study of the degradation process was performed using Response Surface Methodology (RSM) to determine the relationship between the four process variables, namely, initial RhB concentration, NaBH₄ amount, catalyst amount, and time. Optimum points were determined for these four parameters using both matrix and numerical optimization methods. Under optimum conditions, RhB was decolorized with a yield of 98.11%. The apparent activation energy (E_a) and rate constant (k) for the degradation were 24.13 kJ/mol and 0.77 min⁻¹, respectively. The reusability studies of the Ag@PDA@Fe₃O₄@SP exhibited more than 85% degradation ability of the dye even after five cycles. As a result, Ag@PDA@Fe₃O₄@SP possessed high catalytic activity, fast reduction rate, good reusability, easy separation, and simple preparation, endowing this catalyst to be used as a promising catalyst for the decolorization of dyes in aqueous solutions.

Keywords Ag nanoparticles · Decolorization · Fe₃O₄ nanoparticles · Sporopollenin · Rhodamine B · Response Surface Methodology

Introduction

The elimination of organic contaminants in wastewater is a significant subject for environmental and ecological protection. Among organic pollutants, dyestuffs and other

commercial colorants stand out as a focus of environmental improvement efforts (Chirra et al. 2021). Organic dyes used in industries such as paint, textile, plastic, printing, and tanneries have very complex structures. Currently, millions of tons of dyes with different colors are produced worldwide. About 15% of the dyes used in industrial activities are discharged into wastewater as they are not completely fixed (Sen et al. 2011). Most dyes have a complex structure and high chemical stability, making them resistant to photo-degradation, discoloration, and decolorization. The carcinogenic nature of chemically active dyes in industrial wastewater is a major concern. Such dyes cause low photosynthetic activity in water bodies, as they block sunlight and reduce the dissolution of oxygen (Salama et al. 2018). It is possible to remove these pollutants from wastewater chemically, physically, or biologically. Conventional techniques (adsorption, ultrafiltration, coagulation, reverse osmosis, ion exchange, etc.) are used to remove these pollutants (Yılmaz et al. 2019). The dyes in industrial wastewater cause serious

Responsible Editor: Guilherme L. Dotto

✉ Tekin Şahan
tekinsahan@yyu.edu.tr

✉ Adem Zengin
ademzengin@yyu.edu.tr

¹ Department of Chemical Engineering, Institute of Natural and Applied Sciences, Van Yuzuncu Yil University, Van 65080, Turkey

² Faculty of Science, Department of Chemistry, Van Yuzuncu Yil University, 65080 Van, Turkey

³ Faculty of Science, Department of Chemistry, Selcuk University, 42075 Konya, Turkey

environmental pollution because of their high stability and complex structure (Ecer et al. 2021a). Considering all these, the elimination of dye molecules has attracted great interest recently. It is important to search for treatment methods with unique specialties such as no secondary pollution, low cost, high removal efficiency, and easy applicability. The degradation technique, which is one of the removal methods, transforms harmful organic contaminants into lesser detrimental products but does not convert from the water phase to the solid phase, which makes it an efficient technique in preventing and controlling water pollution (Su et al. 2013).

Recently, applications of metal nanoparticles in the field of catalysis are frequently reported. Different materials such as clays, silica gel, biological materials, and activated carbon were used in the degradation process. The support material plays an effective role in providing chemical, thermal, and mechanical stability. As one of these materials, sporopollenin (SP) is very suitable for the modification process due to its high functional group content. SP obtained from *Lycopodium clavatum* is a natural biopolymer containing hydrogen, oxygen, and carbon and has a constant chemical structure. SP has decent stability even after extended exposure to organic and inorganic chemicals (Gubbuk 2011). However, it is difficult to separate biopolymers from water in practical application. To avoid this, researchers recently achieved high recovery by blending them with magnetic materials (Chen et al. 2020). Among diverse materials, iron oxides were extensively examined because they can easily be produced and recovered. Nanoparticles with magnetic properties are promising functional materials for the decolorization and degradation process. Fe_3O_4 , with high stability, superparamagnetic property, and easy recovery, stands out as an important support material (Ecer et al. 2021a; Wang et al. 2018). To enhance the interactions between the active species and the solid support, the support surface can be coated with organic materials or functional polymeric compounds such as polydopamine (PDA) (Ain et al. 2020). The unique wet self-adhesive PDA acts as a binder between support materials and nanocatalysts (Wang et al. 2018). PDA layers have catechol groups in the polymer backbone that can be used for adsorption of metal ions and polymer grafting for in situ nanoparticle synthesis. The surface properties of PDA-coated support materials are becoming popular recently due to their high potential for modification via electrostatic interactions, hydrogen bonding, covalent bonding, and chelation with metal ions (Kumar et al. 2020).

A variety of metal nanoparticles (palladium, platinum, gold, silver, cobalt) can be synthesized for use in the degradation process as catalyst (Li et al. 2017; Mondal et al. 2015). Silver nanoparticles (AgNPs) show promise in having antibacterial and antifouling properties. They are frequently used for catalytic degradation (Deng et al. 2019; Khan et al. 2020; Kumar et al. 2020). PDA can reduce Ag^+ to Ag^0

without the use of any reductants. Most significantly, it was stated that PDA can stick to nearly all material surfaces (Lu et al. 2015). Hence, PDA can be used as a very promising material to coat the surface to allow in situ growth of metal nanoparticles. As far as we know there is no report on PDA-coated magnetic biological material and its implementation for the preparation of Ag NPs.

Traditionally optimization is difficult as it requires a lot of experiments and time. To deal with this, Response Surface Methodology (RSM) has come to the fore as a frequently used optimization method (Ecer et al. 2021a; Şahan and Öztürk 2014). The intended goal is to minimize the number of experiments and to develop a mathematical model to predict response. Optimization with the RSM approach can be described in six phases: (i) choice of independent factors and responses, (ii) choice of design strategy, (iii) application of experiments and acquiring results, (iv) fitting the obtained model equation to experimental data, (v) verification of the model and obtaining response graphs, and (vi) determination of optimum conditions.

In this study, Rhodamine B (RhB), a cationic dye, was selected as the target contaminant. The catalytic decolorization of RhB in the presence of NaBH_4 was chosen to study the catalytic activity of $\text{Ag@PDA@Fe}_3\text{O}_4\text{@SP}$. Various spectroscopic and microscopic analyses were carried out to elucidate the surface properties of the catalyst. Central composite design (CCD) was applied to determine the optimum RhB degradation performance, and also to clarify the relationships between RhB degradation and four related parameters, namely, initial RhB concentration, NaBH_4 amount, catalyst amount, and time.

Materials and method

Material and instruments

Materials and instrument details are given in the Supporting Materials.

Synthesis of magnetic sporopollenin ($\text{Fe}_3\text{O}_4\text{@SP}$) composite

$\text{Fe}_3\text{O}_4\text{@SP}$ was synthesized in a similar manner to the previously published procedure (Chen et al. 2017). The magnetic SP was prepared by an in situ growth method, in which Fe_3O_4 nanoparticles were nucleated on the SP surface by coprecipitating ferrous (Fe^{+2}) and ferric (Fe^{+3}) ion solutions. Firstly, a solution of $\text{FeCl}_3 \cdot 6\text{H}_2\text{O}$ (0.305 g) and $\text{FeCl}_2 \cdot 4\text{H}_2\text{O}$ (0.112 g) in 10 mL deionized water was prepared. Then, 0.5 mL of NH_4OH was added to this solution and then 0.1 g of SP was quickly added to the mixture and the temperature was brought to 90° . After half an hour, it was collected with

the help of a magnet and washing was continued until the pH value was neutral. It was then dried at 60° for 24 h.

Synthesis of PDA@Fe₃O₄@SP composite

To polymerize the surface of the Fe₃O₄@SP with PDA, 0.1 g Fe₃O₄@SP was mixed in 50 mL of Tris buffer (10 mM, pH 8.5) containing 1 mg/mL dopamine hydrochloride at 750 rpm on a mechanical stirrer for 18 h. The obtained polymeric particles were collected with a magnet and washed and then dried at 60 °C for 24 h to obtain PDA@Fe₃O₄@SP.

Synthesis of Ag@PDA@Fe₃O₄@SP composite

Then, silver nanoparticles were deposited on PDA@Fe₃O₄@SP. For this purpose, PDA-coated Fe₃O₄@SP samples were mixed in AgNO₃ aqueous solution in a shaker at 25 °C for 24 h. After washing, the samples were dried at 60 °C for 12 h. The final product was named Ag@PDA@Fe₃O₄@SP. The overall synthetic procedure is schematically given in Fig. 1.

Determination of catalytic activity

The catalytic activity of Ag@PDA@Fe₃O₄@SP was appraised for the degradation of RhB. All experiments were performed considering the parameters with ranges and levels that are given in Table 1. The concentration of RhB before and after the experimental procedure was detected via UV–Vis spectroscopy at $\lambda_{\max} = 553$ nm. The following equation was used to obtain % degradation.

$$\text{Degradation\%} = \frac{(C_o - C_e)}{C_o} \times 100 \quad (1)$$

where C_o is the initial and C_e is the equilibrium concentration of dye, respectively.

For the stability and reusability of the synthesized catalyst, the decolorization process was completed at optimum conditions. After each cycle, the catalyst was washed with ethyl alcohol and filtered with the help of magnet, and then dried at 60 °C for use in the next cycle. This process was continued until five cycles were completed.

Fig. 1 Schematic representation of Ag@PDA@Fe₃O₄@SP synthesis

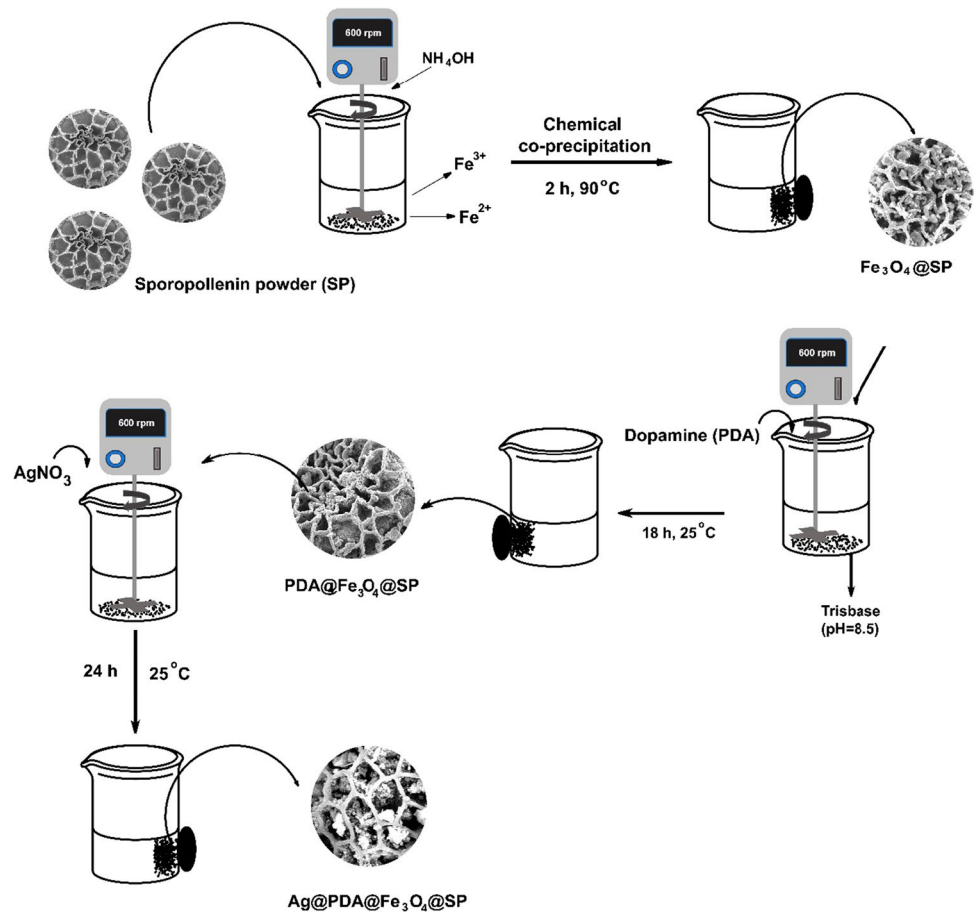


Table 1 Independent variable factors and levels, CCD experiments, and obtained responses

Parameters	Units	Parameter code	Level and range (coded)		
			− 1	0	1
Initial dye concentration	mg/L	X_1	10	30	50
NaBH ₄ amount	M	X_2	0.05	0.275	0.5
Catalyst amount	mg/mL	X_3	0.1	0.55	1
Contact time	min	X_4	0.5	1.75	3
Run	X_1	X_2	X_3	X_4	Degradation %
1	50	0.05	1	3	75.04
2	50	0.5	1	0.5	85.50
3	10	0.5	0.1	3	83.50
4	30	0.275	0.55	3	97.60
5	10	0.05	1	3	76.00
6	30	0.05	0.55	1.75	85.90
7	30	0.5	0.55	1.75	92.50
8	50	0.5	1	3	84.70
9	30	0.275	1	1.75	92.53
10	50	0.5	0.1	3	82.38
11	10	0.05	0.1	3	84.20
12	30	0.275	0.55	1.75	97.67
13	30	0.275	0.1	1.75	92.90
14	50	0.05	0.1	0.5	77.50
15	10	0.275	0.55	1.75	89.50
16	10	0.5	1	0.5	79.90
17	50	0.05	0.1	3	85.70
18	10	0.5	1	3	83.90
19	10	0.05	0.1	0.5	70.50
20	50	0.5	0.1	0.5	80.84
21	30	0.275	0.55	1.75	97.67
22	30	0.275	0.55	1.75	97.92
23	30	0.275	0.55	1.75	98.05
24	30	0.275	0.55	1.75	97.88
25	50	0.275	0.55	1.75	90.98
26	30	0.275	0.55	1.75	98.00
27	10	0.05	1	0.5	68.50
28	50	0.05	1	0.5	72.10
29	30	0.275	0.55	0.5	89.50
30	10	0.5	0.1	0.5	74.60

Experimental design and optimization

The effects of different parameters affecting degradation were investigated using an experimental design approach. For this, RSM with a central composite design (CCD) was performed. The levels and ranges of these parameters are given in Table 1. RSM suggested 30 experiments that should be performed for four independent parameters. A second-order polynomial equation was used to evaluate the obtained experimental results. This equation can be

obtained as quadratic or linear equation. The correlation between response and independent parameters is given in Eq. (2).

$$y_p = \beta_0 + \sum_{i=1}^k \beta_i x_i + \sum_{i=1}^k \beta_{ii} x_i^2 + \sum_{i=1}^k \sum_{j=i+1}^k \beta_{ij} x_i x_j \quad (2)$$

where y_p represents the results to be optimized; x_i indicates the studied variable; β_0 , β_i , and β_{ij} are the regression coefficients; and finally, the number of parameters is denoted by k .

Results and discussion

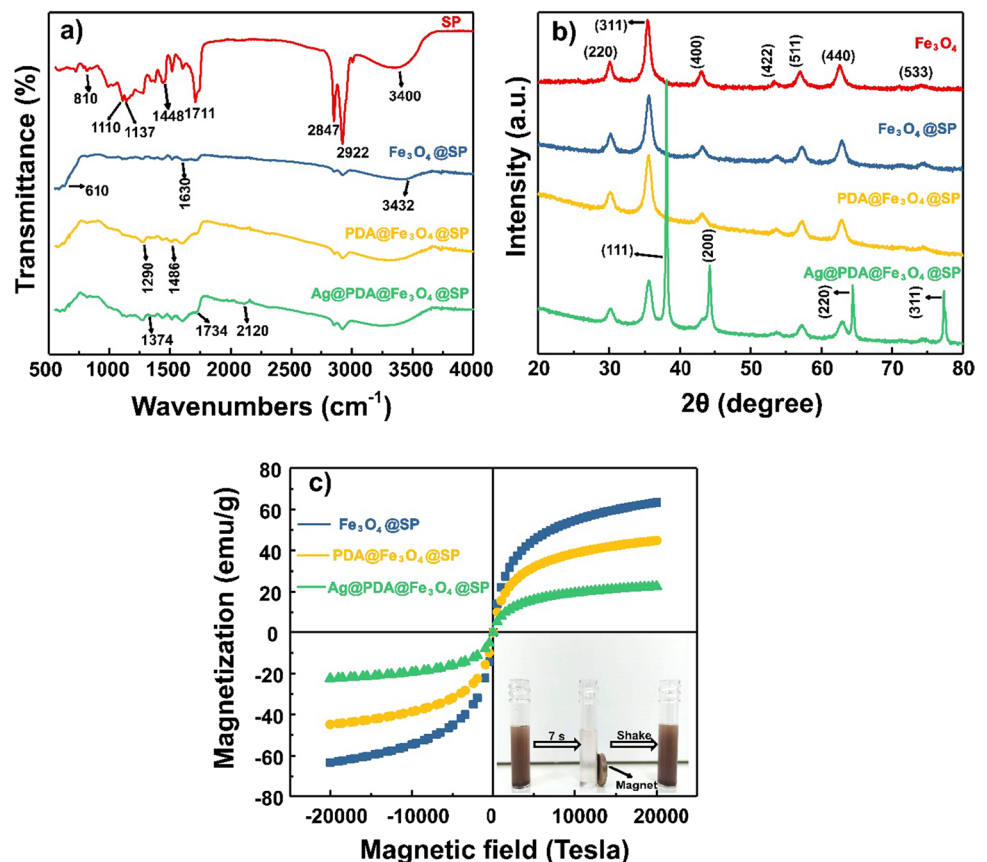
Characterization of particles

ATR-FTIR spectroscopy was carried out to reveal the functional groups within the structure of SP, Fe_3O_4 @SP, PDA@ Fe_3O_4 @SP, and Ag@PDA@ Fe_3O_4 @SP (Fig. 2a). For SP, the peak at 3400 cm^{-1} was attributed to the OH stretching frequency of the surface and also to adsorbed water molecules (Baran et al. 2017). The peaks at 2922 and 2847 cm^{-1} were due to C–H symmetric stretching (Ahmad et al. 2017; Gubbuk 2011). The peak seen at 1448 cm^{-1} was due to the C=C stretching vibration of aromatic rings and the C=O stretching vibration of a carboxylic group was present at 1711 cm^{-1} (Ahmad et al. 2017). The characteristic absorption bands at 1033 cm^{-1} and 1010 cm^{-1} were C–N stretching vibrations and C–O stretching vibrations in polysaccharides or polysaccharide-like substances, respectively (Dyab et al. 2016). For Fe_3O_4 @SP, the intense peak observed at 610 cm^{-1} was attributed to the stretching vibration mode related to the metal–oxygen Fe–O bonds in the crystalline lattice of Fe_3O_4 . They are characteristically evident for all spinel structures and particularly ferrites. The broad peak centered at 3435 cm^{-1} and a peak at

1629 cm^{-1} were due to the presence of –OH groups and to OH stretching and OH bending, respectively (Nalbandian et al. 2016). After polymerization, a new absorbance peak at 1290 cm^{-1} emerged, which was attributed to the phenolic C–OH stretching vibration of PDA (Touqeer et al. 2020). Finally, absorption peaks at 1734 and 1374 cm^{-1} indicated the presence of Ag^0 nanoparticles (Jyoti et al. 2016).

The crystal structure of each magnetic sample was investigated by XRD. Compared with pristine Fe_3O_4 nanoparticles (Fig. 2b), magnetic nanoparticles loaded with SP showed the same diffraction lines recorded at $2\theta = 30.13^\circ$, 35.36° , 43.05° , 53.20° , 56.95° , and 62.55° , corresponding to (220), (311), (400), (422), (511), and (440), respectively (JCPDS Card: 19–0629) (Uzuriaga-Sánchez et al. 2016), implying the spinel structure of magnetic nanoparticles. In addition, the crystalline structure was preserved after coating the PDA layer onto Fe_3O_4 @SP (Fig. 2b), indicating that the coating by PDA was non-destructive. Apart from the diffraction lines of magnetic nanoparticles, different diffraction lines appeared at $2\theta = 38.05^\circ$, 44.17° , 64.33° , and 77.32° , which were indexed as (111), (200), (220), and (311), respectively. The new diffraction lines matched the face-centered cubic crystallographic structure of silver nanoparticles (JCDPS Card: 84–0713) (Vanaja and Annadurai

Fig. 2 (a) ATR-FTIR, (b) XRD, and (c) VSM loops of synthesized particles



2013). The particle size of the deposited Fe_3O_4 and Ag NPs on SP was calculated to be 17.94 nm and 31.06 nm, respectively, using Debye–Scherrer equation (Das et al. 2018). The results clearly show successful deposition of the silver nanoparticles.

Magnetization behavior and saturation magnetization (M_s) values of each magnetic sample were examined by VSM. Figure 2c presents the magnetic hysteresis loops of the samples at room temperature which passed through the origin indicating the superparamagnetic characteristics of the samples. The M_s Fe_3O_4 @SP, PDA@ Fe_3O_4 @SP, and Ag@PDA@ Fe_3O_4 @SP were 65.3, 46.3, and 21.4 emu/g, respectively. The M_s value of Ag@PDA@ Fe_3O_4 @SP seemed sufficient for fast magnetic separation applications (Ecer et al. 2021b; Hassan et al. 2020).

The surface morphology of each sample was investigated by SEM and corresponding low- and high-magnification SEM photomicrographs are shown in Fig. 3. Raw SP had nearly smooth spherical morphology with interconnected and uniform pore structures, as shown in Fig. 3a. After deposition of Fe_3O_4 nanoparticles, the surface of SP became more porous and Fe_3O_4 nanoparticles were predominantly located on pore walls of SP, as shown in the high-magnification SEM photomicrograph (Fig. 3b). After coating of PDA on Fe_3O_4 @SP, the morphology is almost unchanged, most probably due to the grafting of a very thin layer of PDA (Ball 2018; Kohri et al. 2013). However, the morphology of PDA@ Fe_3O_4 @SP changed dramatically and the roughness of the surface increased as a result of loading of Ag nanoparticles.

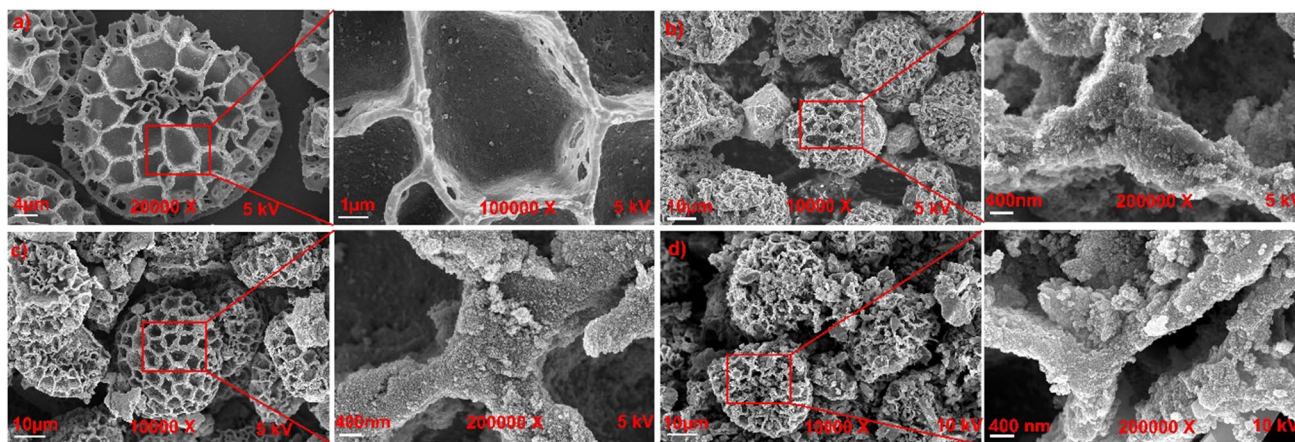


Fig. 3 SEM images of (a) SP, (b) Fe_3O_4 @SP, (c) PDA@ Fe_3O_4 @SP, and (d) Ag@PDA@ Fe_3O_4 @SP

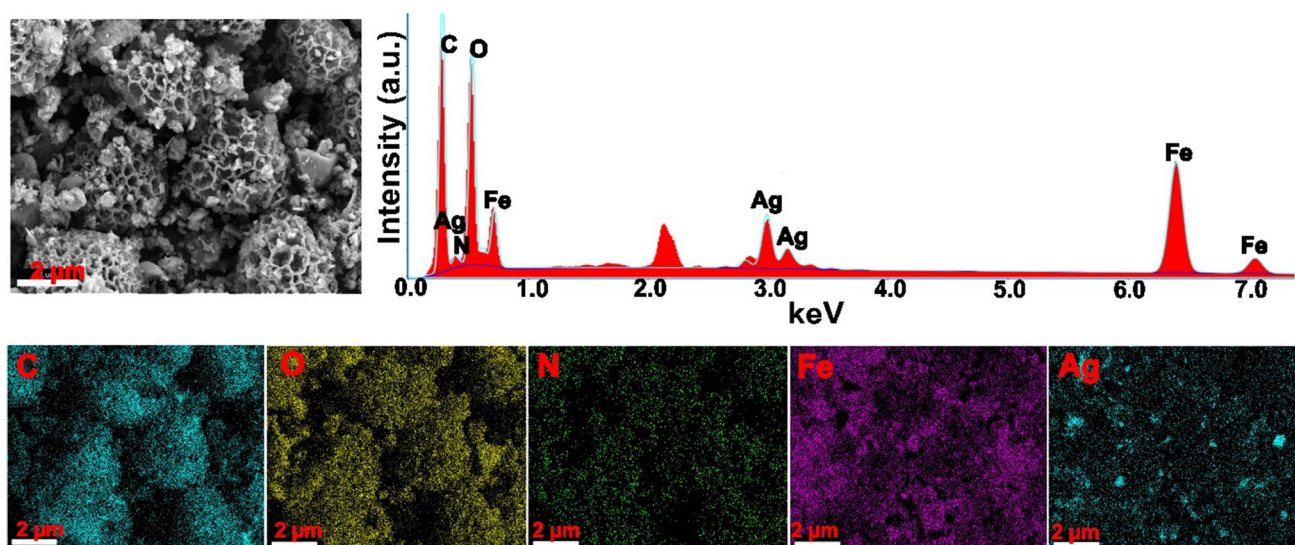
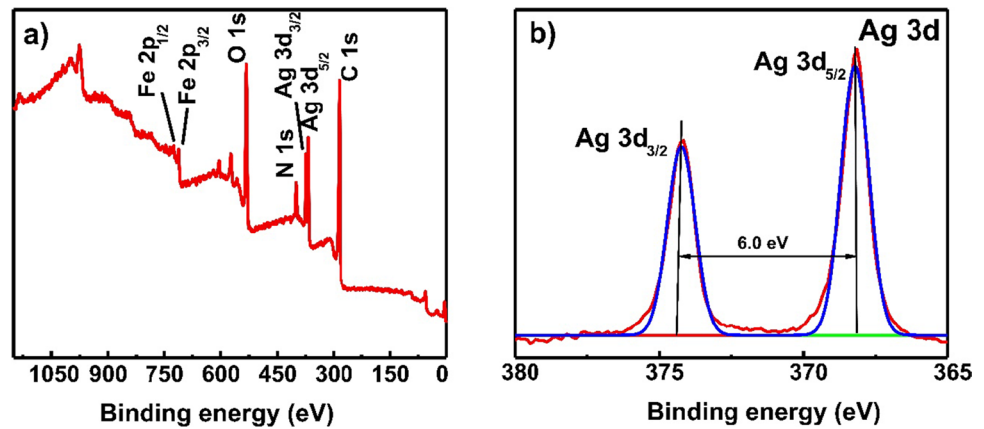


Fig. 4 EDX spectrum and elemental analysis of Ag@PDA@ Fe_3O_4 @SP

Fig. 5 X-ray photoelectron spectroscopy (XPS) analysis of Ag@PDA@Fe₃O₄@SP: (a) survey spectrum and (b) core level of Ag 3d spectrum



Moreover, the deposition of Ag nanoparticles onto PDA@Fe₃O₄@SP was also investigated by SEM–EDX and elemental mapping. As presented in Fig. 4, the EDX spectrum of Ag@PDA@Fe₃O₄@SP showed Ag peaks apart from C, O, N, and Fe. Elemental mapping of the sample also revealed that Ag nanoparticles were homogeneously distributed on the PDA@Fe₃O₄@SP.

To further verify the deposition of Ag nanoparticles, XPS analysis was carried out and the corresponding survey and core-level XPS spectra for Ag@PDA@Fe₃O₄@SP are given in Fig. 5. As shown in the XPS survey scan (Fig. 5a), apart from Fe, O, N, and C elemental peaks, Ag elemental peaks were also recorded which matched the SEM–EDX spectrum well, indicating the successful deposition of Ag nanoparticles onto PDA@Fe₃O₄@SP. Moreover, the core-level XPS spectra of Ag 3d (Fig. 5b) can be divided into two peaks recorded at 372.9 eV and 366.9 eV attributed to Ag 3d_{3/2} and Ag 3d_{5/2}, respectively. In addition, the spin orbit splitting energy of the Ag 3d doublet was 6.0 eV, indicating that the deposited silver nanoparticles were zero-valent (Kong and Jang 2008). The calculated relative atomic concentration of Ag based on Ag 3d was 2.4%.

Optimization for degradation of RhB

Experimental conditions for the catalytic reduction of RhB using catalyst Ag@PDA@Fe₃O₄@SP in the presence of NaBH₄ as a reduction agent were optimized using RSM. As shown in Table 1, a three-level CCD was used to optimize the effect of parameters on the response variant using RSM. The quadratic model equation obtained after the experiments is given in Eq. (3). Considering all possible combinations, RSM proposed a total of 30 experiments for the four variables for optimization of the data. The significance of all the parameters for the response were approximated using the analysis of variance (ANOVA) approach.

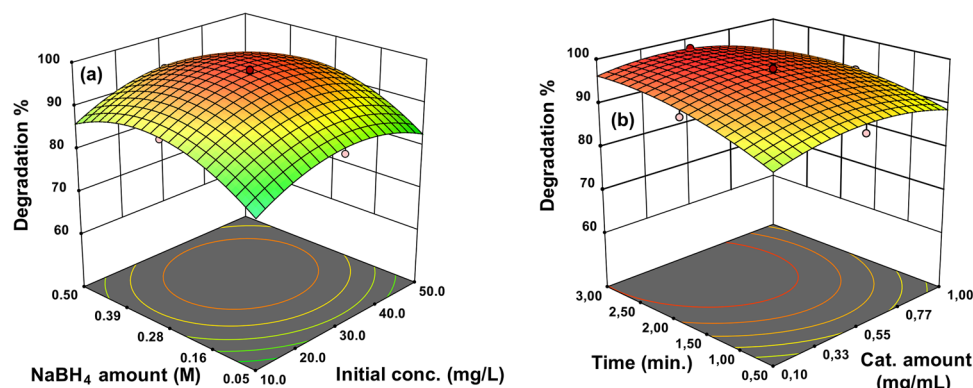
$$\begin{aligned} \text{Degradation\%} = & 52.07749 + 1.031814(X_1) + 79.79836(X_2) \\ & + 13.64116(X_3) + 11.65701(X_4) \\ & + 0.005278(X_1X_2) - 0.03181(X_1X_3) \\ & - 0.05555(X_1X_4) + 24.03704(X_2X_3) - 4.15556(X_2X_4) \\ & - 2.07778(X_3X_4) - 0.01419(X_1^2) - 132.675(X_2^2) \\ & - 15.8026(X_3^2) - 1.51469(X_4^2) \end{aligned} \quad (3)$$

The significance of the model obtained for RhB degradation yield was completely checked by performing ANOVA. The obtained quadratic model statistics and ANOVA conclusions are given in Table S1. It is obvious that with high *F*-value (108.64) and low *p*-value (<0.0001), the suggested quadratic model is significant and had good fit. Also, the high correlation coefficient ($R^2=0.99$) indicates a model with good fit (Bose et al. 2021).

The graphs in Fig. S1 give the relationship between the residual values and the actual value. The results obtained from the proposed quadratic equation (predicted) and the experimental results (actual) are in high agreement (Fig. S1a). Additionally, the residuals were compared with the predicted results to analyze the error distribution. The plot of predicted values against externally studentized residuals in Fig. S1b shows that all points have random spread and are located within the limits in the range between ± 4 . Therefore, it is clearly seen that the model suggested by RSM is a suitable tool for estimating the degradation process (Bose et al. 2021).

The 3D graphs produced by RSM were evaluated to observe the effects of the studied independent factors for the degradation of RhB (Fig. 6). To examine the effect of the initial RhB concentration, the range from 10 to 50 mg/L was studied. In Fig. 6a, the degradation yield of RhB initially increases with increasing C_o . The presumed cause is that when the C_o of RhB rises, sufficient active sites are available on the Ag@PDA@Fe₃O₄@SP surface. After a certain increase, it is observed that the degradation yield decreases. Since the amount of NaBH₄ and catalyst

Fig. 6 The 3-dimensional surface plots of the effect of (a) NaBH_4 amount and initial RhB concentration and (b) catalyst amount and contact time



in the solution are constant, the maximum amount of dye that can be degraded is limited. Therefore, it is usual for increased RhB concentration to decrease the degradation yield (Li et al. 2019).

Also in Fig. 6a, the effect of the NaBH_4 amount on the degradation efficiency can also be examined. Increasing NaBH_4 amount at the beginning increases the degradation efficiency. As a hydrogen source, NaBH_4 is catalytically decomposed by Ag NPs to release hydrogen atoms. The hydrogens obtained as a result of decomposition react with RhB molecules and result in their decomposition into CO_2 , H_2O , and other small molecules (Li et al. 2019). During the degradation process, firstly dye molecules and BH_4^- diffuse from the aqueous solution to the $\text{Ag@PDA@Fe}_3\text{O}_4\text{@SP}$ surface. Ag NPs on the catalyst surface act as the electron relay system to accelerate electron transfer from the BH_4^- to the RhB (Mishra et al. 2016). The NaBH_4 amount reached maximum efficiency at about 0.3 M. When the NaBH_4 amount increased more than 0.3 M, a decrease in the degradation efficiency was observed (Fig. 6a). The possible reason for this is that with the increasing amount of NaBH_4 , more hydrogen was produced and adhered to the catalyst surface. It caused a decrease in the degradation rate of RhB due to the lower amount of dye molecules compared to hydrogen adsorbed on the catalyst surface (Naseem et al. 2019).

The effect of $\text{Ag@PDA@Fe}_3\text{O}_4\text{@SP}$ catalyst amount on the decolorization was investigated and given in Fig. 6b. Degradation yield increased with an increase in catalyst amount up to approximately 0.45 mg/mL. Further increments in catalyst dosage led to a decrease in decolorization yield. The initial increase in yield can be interpreted as an increase in the number of active sites on the $\text{Ag@PDA@Fe}_3\text{O}_4\text{@SP}$ surface as a result of increased dosage. The subsequently observed decrease in degradation efficiency can be explained by the fact that the suspended particles increase further as the catalyst dosage increases beyond the optimum

(Aisien et al. 2013). Therefore, the catalyst surface area is reduced, which leads to a reduction in the active sites, and as a result, the efficiency decreases.

Finally, experiments were carried out in the range of 0.5–3 min to determine the effect of reaction time. The degradation yield of RhB increased with reaction time and achieved maximum yield after approximately 2.5 min (Fig. 6b). The high catalytic activity, short reduction time, recycling, and easy separation were significant benefits of $\text{Ag@PDA@Fe}_3\text{O}_4\text{@SP}$ for use as an effective and recyclable catalyst for the degradation of RhB in wastewater.

Process optimization and confirmation of the model

The main reason for performing optimization is to define the optimal points of the factors affecting the response. In order to define the optimum values of the parameters, optimum conditions can be obtained with the matrix method by using the model equation (Eq. (3)) suggested by the model (Şahan and Öztürk 2014). A general solution can be acquired from Eq. (4). If the second-order model is written in matrix notation,

$$y = \beta_0 + x^t b + x^t B x_s \quad (4)$$

where

$$x_s = \begin{bmatrix} X_1 \\ X_2 \\ X_k \end{bmatrix}, b = \begin{bmatrix} \beta_1 \\ \beta_2 \\ \beta_k \end{bmatrix} \text{ and } B = \begin{bmatrix} \beta_{11} & \beta_{12}/2 & \beta_{1k}/2 \\ \text{sym} & \beta_{22} & \beta_{2k}/2 \\ \text{sym} & \text{sym} & \beta_{kk} \end{bmatrix}$$

where b and B are the matrices obtained from the coefficients in Eq. (3). The constant points (X_s) are obtained from the solution of Eq. (5).

$$x_s = -\frac{1}{2} B^{-1} b \quad (5)$$

The optimum points to maximize the % degradation were evaluated by application of Eq. (4).

$$x_s = \begin{bmatrix} C_o \\ \text{NaBH}_4 \text{ amount} \\ \text{Catalyst amount} \\ \text{Time} \end{bmatrix}, b = \begin{bmatrix} 1.031814 \\ 79.79836 \\ 13.64116 \\ 11.65701 \end{bmatrix}, \text{ and}$$

$$B = \begin{bmatrix} -0.01419 & 0.005278/2 & -0.03181/2 & -0.0555/2 \\ \text{syn} & -132.675 & 24.037/2 & -4.155/2 \\ \text{syn} & \text{syn} & -15.8026 & -2.077/2 \\ -\text{syn} & \text{syn} & \text{syn} & -1.51469 \end{bmatrix}$$

When these matrices are solved according to Eq. (5), the following matrix is obtained.

$$x_s = \begin{bmatrix} 30.90 \\ 0.304 \\ 0.460 \\ 2.540 \end{bmatrix}$$

The optimum values for RhB degradation from the solution of the above matrices are 30.9 mg/L for Co, 0.304 M for the amount of NaBH₄, 0.46 mg/mL for amount of catalyst, and 2.54 for time. The same values were obtained by using the numerical optimization method in RSM. Under these optimum values, the degradation value was obtained as 98.11%. These results were confirmed by experiments.

The degradation of different dyes, Malachite green (MG), Reactive orange (RO), Methyl orange (MO), Coomassie brilliant blue (CBB), and Methyl red (MR), was investigated under optimum conditions obtained for RhB. The degradation yields for RO, CBB, MG, MR, and MO dyes were obtained as 58.4%, 59.6%, 80.1%, 71.7%, and 86.7%, respectively (Fig. S2). These results show that Ag@PDA@Fe₃O₄@SP catalyst has high catalytic effect for different dyes as well as for degradation of RhB dye (98.11%). In line

with these results, it can be said that Ag@PDA@Fe₃O₄@SP is an efficient catalyst for the degradation process.

Additionally, SP, Fe₃O₄@SP, and PDA@Fe₃O₄@SP materials were used as catalysts in degradation of RhB to better understand the importance of Ag@PDA@Fe₃O₄@SP. The UV–Vis spectra obtained initially and at the end of the RhB degradation using these materials are given in Fig. 7a. The % decolorization obtained using SP, Fe₃O₄@SP, and PDA@Fe₃O₄@SP under optimum conditions were obtained as 5.6, 18.9, and 62.4, respectively (Fig. 7b). The degradation efficiency obtained using Ag@PDA@Fe₃O₄@SP (98.3%) is higher than the yield obtained for these materials. Consequently, it can be said that Ag@PDA@Fe₃O₄@SP is an effective catalyst due to having higher efficiency than SP, Fe₃O₄@SP, and PDA@Fe₃O₄@SP and being easily degradable, environmentally friendly, and easy to synthesize.

A comparison table was added to compare the catalytic performance of the synthesized Ag@PDA@Fe₃O₄@SP catalyst with materials previously used for RhB degradation (Table 2). Ag@PDA@Fe₃O₄@SP was observed to show unique or similar catalytic activity compared to the materials given in the table. The synthesized catalyst is an effective catalyst due to benefits such as being easy to synthesize, efficient, and easy to separate.

Kinetic and thermodynamic analyses for degradation of RhB

Experimental data were applied to pseudo-first-order (PFO) kinetic equations under the obtained optimum conditions to better understand the control mechanism throughout the degradation process. The degradation efficiency increased with elongated reaction time. The reaction was in good agreement with the PFO model. The correlation between ln C_t/C_o and

Fig. 7 RhB degradation with SP, Fe₃O₄@SP, PDA@Fe₃O₄@SP, and Ag@PDA@Fe₃O₄@SP under the optimum conditions: (a) UV–Vis spectra and (b) decolorization %

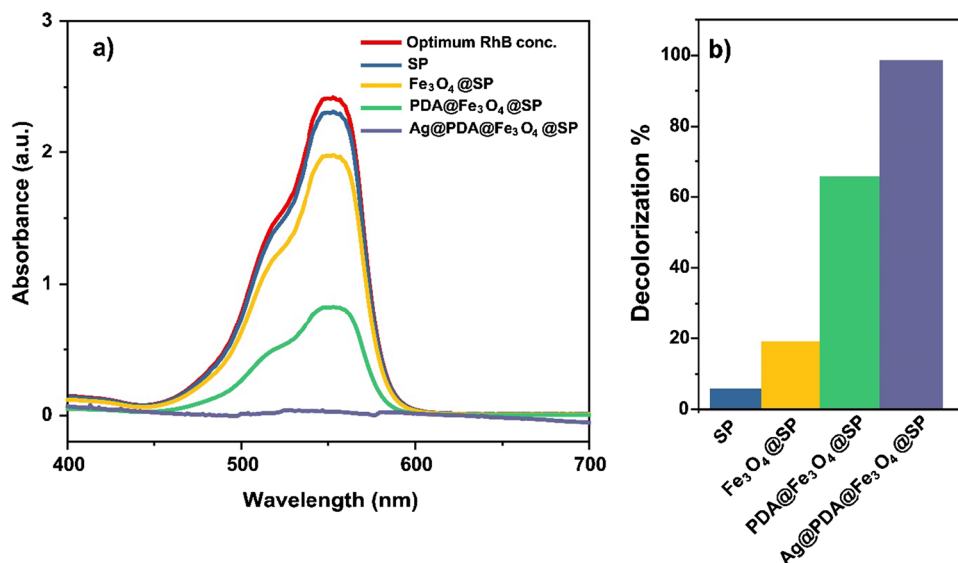


Table 2 Comparison of Ag@PDA@Fe₃O₄@SP as nanocatalyst with those reported in the literature for RhB degradation

Catalyst	C_o (mg/L)	Catalyst amount (mg/mL)	NaBH ₄ amount	k (min ⁻¹)	Ref
CoFe ₂ O ₄ -P4VP@Ag NPs	20	0.2	10 mM	0.26	Li et al. (2020a)
ZIF-8	5	1	8 mM	-	Chirra et al. (2021)
Porous Cu microspheres	70	0.012	6.25 mM	0.81	Zhang et al. (2014)
Pt/Ag nanoparticles	4	0.216	2 mM	0.49	Kim et al. (2011)
AgNPs@PAN/GO-SH	10	0.4	0.1 M	0.26	Li et al. (2020b)
Cu-Ni	20	2.85	0.07 M	0.38	Ismail et al. (2018)
Ni/CPM	15	0.285	10 mM	0.47	Veerakumar et al. (2015)
Ag-Fe ₃ O ₄ composite	20	0.74	50 mM	0.42	Ai et al. (2011)
Ag@PDA@Fe ₃ O ₄ @SP	30.9	0.46	0.304 M	0.77	This study

the reaction time was linear. The PFO kinetic equation can be given as follows:

$$\ln\left(\frac{C_t}{C_o}\right) = -kt \quad (6)$$

where C_t and C_o are the RhB concentration at time t and initially, respectively. k (min⁻¹) is the PFO rate constant and t is the reaction time. The variation of RhB concentration with time at 553 nm and the linear plot of $\ln(C_t/C_o)$ versus t are given in Fig. S3. The rate constant (k) for the degradation process of RhB by Ag@PDA@Fe₃O₄@SP was obtained as 0.774 min⁻¹.

In addition, the effect of temperature on RhB degradation was investigated under the optimum conditions. Increasing temperature had a positive effect on the RhB degradation efficiency. According to the kinetic rate constant (k) at different temperatures (25–60 °C), the apparent activation energy for RhB degradation by Ag@PDA@Fe₃O₄@SP was computed using the Arrhenius equation:

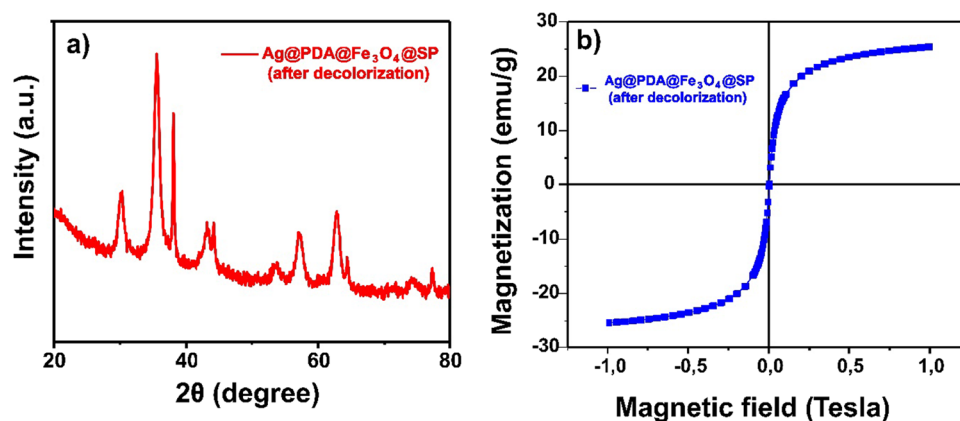
$$\ln k = -\frac{E_a}{RT} + \ln A \quad (7)$$

where A is the pre-exponential factor, E_a (J/mol) is the apparent activation energy, R (8.314 J/mol·K) is the ideal gas constant, and T (K) is the absolute temperature. The linear plot of $\ln(k)$ versus $1/T$ is given in Fig. S4. E_a was obtained as 24.13 kJ/mol.

Recyclability of catalyst

The reusability and stability of the synthesized nanomaterial were examined for up to five cycles for RhB decolorization in the presence of NaBH₄. After each cycle, Ag@PDA@Fe₃O₄@SP was separated from the reaction mixture with a magnet, washed with ethyl alcohol, and used in the next cycle. It was observed that the %degradation of RhB by the regenerated catalyst was not significantly reduced compared to the fresh catalyst after five cycles (Fig. S5). Furthermore, XRD and VSM analyses of Ag@PDA@Fe₃O₄@SP after five cycles of the decolorization process are presented in Fig. 8. It could be clearly seen that the XRD pattern of the reused Ag@PDA@Fe₃O₄@SP (Fig. 8a) was similar to that of the fresh sample (see Fig. 2b), suggesting that Ag@PDA@Fe₃O₄@SP possessed high structural stability. Moreover, the magnetic properties of Ag@PDA@Fe₃O₄@SP have not changed significantly even after five cycles. The M_s of

Fig. 8 (a) XRD pattern of Ag@PDA@Fe₃O₄@SP after decolorization and (b) VSM curve of Ag@PDA@Fe₃O₄@SP after decolorization



Ag@PDA@Fe₃O₄@SP was obtained as 25.77 emu/g after the decolorization process (Fig. 8b). The M_s value of Ag@PDA@Fe₃O₄@SP before decolorization was 21.4 emu/g (see Fig. 2c). Moreover, Ag content of the catalyst was determined by ICP-MS. The obtained results showed that it decreased from 11.79 to 9.16% after five cycles. The fact that non-magnetic Ag NPs passed from the catalyst to the solution confirms the increased of M_s value. Also, the small decrease in efficiency can be attributed to the loss of active Ag nanoparticles on the catalyst surface during the washing process.

Possible degradation mechanism

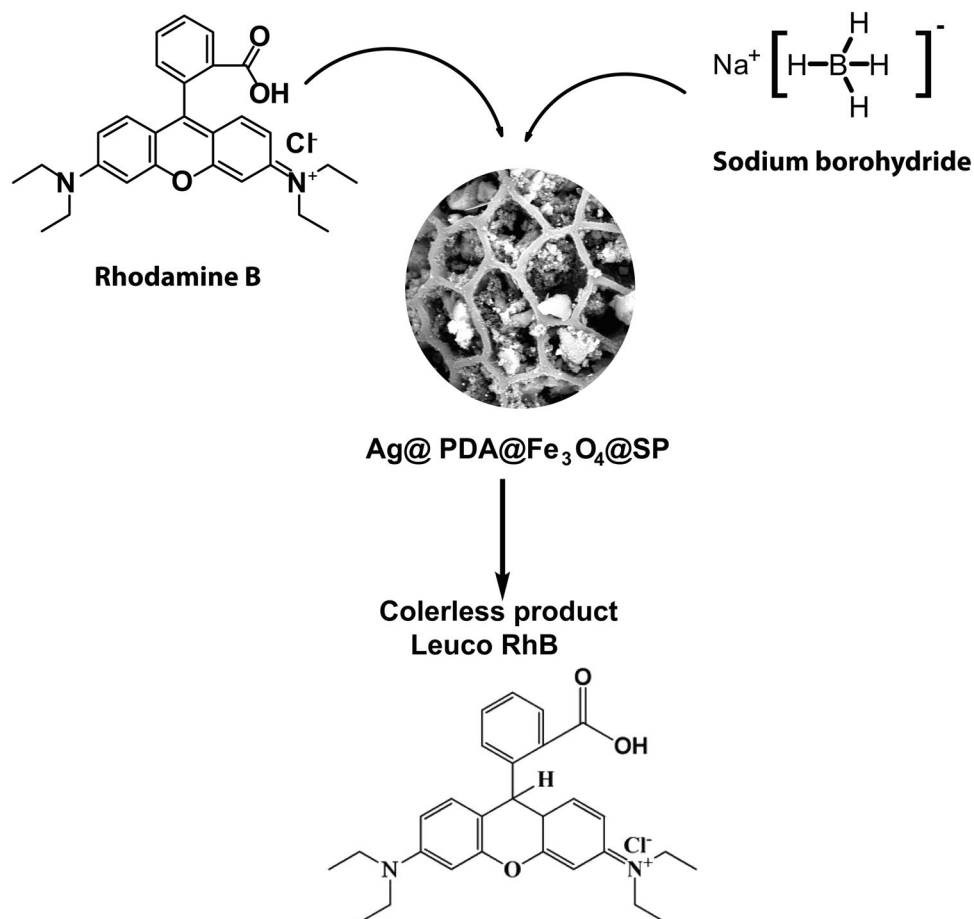
The possible decolorization mechanism for RhB degradation using Ag@PDA@Fe₃O₄@SP as a novel polymeric catalyst is given schematically in Fig. 9. The catalyst activity relies directly on the electron agreement capability of the dye molecule and the electron donation capability of NaBH₄. For the catalytic reduction of RhB, Ag NPs on the catalyst surface (Ag@PDA@Fe₃O₄@SP) act as an electron relay system (Jeyapragasam and Kannan 2016). Initially, dye molecules and NaBH₄ are absorbed onto the Ag@PDA@Fe₃O₄@SP surface. Next, the dye molecule behaves like an electrophilic

agent, and NaBH₄ as a nucleophilic agent. Ag@PDA@Fe₃O₄@SP behaves as a relay system and helps in transferring the electron required for the dye degradation process from NaBH₄ to the dye molecule (Gola et al. 2021). The uptake of electrons readily led to the decolorization of RhB by an oxidation–reduction reaction. Thus, it results in the degradation of the RhB chromophore structure to a colorless product (Leuco RhB) (He et al. 2019; Kurtan et al. 2016).

Conclusion

As a result, Ag@PDA@Fe₃O₄@SP, a highly effective magnetic hybrid catalyst, was synthesized using an easy and economical synthesis protocol and provided great dye decolorization ability in the presence of NaBH₄. Ag@PDA@Fe₃O₄@SP was characterized by FT-IR, SEM, XRD, XPS, ICP-MS, and VSM techniques. RSM was applied to optimize variables for the degradation of RhB using Ag@PDA@Fe₃O₄@SP nanoparticles in the presence of NaBH₄. A quadratic model revealed the functional relationship between %degradation and four independent variables. Under the optimized conditions, the degradation efficiency of RhB was 98.11%. A high R^2 value of

Fig. 9 Possible decolorization mechanism



0.9902 was found indicating sufficient agreement between the experimental and predicted results. The apparent activation energy (E_a) and reaction rate constant (k) were 24.13 kJ/mol and 0.77 min^{-1} , respectively. Reusability studies showed high activity of Ag@PDA@Fe₃O₄@SP in the decolorization of RhB even after five cycles. Consequently, it can be said that Ag@PDA@Fe₃O₄@SP is a good choice as a nanocatalyst for the degradation of toxic dyes in aqueous media.

Supplementary Information The online version contains supplementary material available at <https://doi.org/10.1007/s11356-022-21416-2>.

Author contribution Ümit Ecer: investigation, data analysis, material synthesis and characterization, writing—original draft preparation, and experiments. Tekin Şahan: data analysis, experiments, methodology, material synthesis and characterization, writing—reviewing and editing. Adem Zengin: data analysis, experiments, methodology, material synthesis and characterization, writing—reviewing and editing. İlkey Hilal Gübbük: investigation and data analysis.

Availability of data and materials Not applicable.

Declarations

Ethics approval The authors all agree to ethical approval and understand its related rules and content.

Consent to participate The authors of this manuscript are all aware of the journal to which the manuscript was submitted, and all agree to continue to support the follow-up work.

Consent for publication This manuscript has not been submitted or published in other journals, and the authors agree to consent to publish.

Conflict of interest The authors declare no competing interests.

References

- Ahmad NF, Kamboh MA, Nodeh HR, Halim SNBA, Mohamad S (2017) Synthesis of piperazine functionalized magnetic sporopollenin: a new organic-inorganic hybrid material for the removal of lead(II) and arsenic(III) from aqueous solution. *Environ Sci Pollut Res* 24:21846–21858. <https://doi.org/10.1007/s11356-017-9820-9>
- Ai L, Zeng C, Wang Q (2011) One-step solvothermal synthesis of Ag-Fe₃O₄ composite as a magnetically recyclable catalyst for reduction of Rhodamine B. *Catal Commun* 14:68–73. <https://doi.org/10.1016/j.catcom.2011.07.014>
- Ain QU, Rasheed U, Yaseen M, Zhang H, Tong Z (2020) Superior dye degradation and adsorption capability of polydopamine modified Fe₃O₄-pillared bentonite composite. *J Hazard Mater* 397:122758. <https://doi.org/10.1016/j.jhazmat.2020.122758>
- Aisien F, Amenaghawon N, Ekpenisi E (2013) Photocatalytic decolorisation of industrial wastewater from a soft drink company. *J Eng Appl Sci* 9:11–16
- Ball V (2018) Polydopamine nanomaterials: recent advances in synthesis methods and applications. *Front Bioeng Biotechnol* 6. <https://doi.org/10.3389/fbioe.2018.00109>
- Baran T, Sargin I, Kaya M, Menteş A, Ceter T (2017) Design and application of sporopollenin microcapsule supported palladium catalyst: remarkably high turnover frequency and reusability in catalysis of biaryls. *J Colloid Interface Sci* 486:194–203. <https://doi.org/10.1016/j.jcis.2016.09.071>
- Bose S, Kumar Tripathy B, Debnath A, Kumar M (2021) Boosted sono-oxidative catalytic degradation of Brilliant green dye by magnetic MgFe₂O₄ catalyst: degradation mechanism, assessment of bio-toxicity and cost analysis. *Ultrason Sonochem* 75:105592. <https://doi.org/10.1016/j.ultsonch.2021.105592>
- Chen H, Li Y, Wang S, Zhou Y (2017) Synthesis of montmorillonite/Fe₃O₄-OTAB composite capable of using as anisotropic nanoparticles. *Appl Surf Sci* 402:384–391. <https://doi.org/10.1016/j.apsusc.2017.01.103>
- Chen B, Long F, Chen S, Cao Y, Pan X (2020) Magnetic chitosan biopolymer as a versatile adsorbent for simultaneous and synergistic removal of different sorts of dyestuffs from simulated wastewater. *Chem Eng Sci* 385:123926. <https://doi.org/10.1016/j.ces.2019.123926>
- Chirra S, Wang L-F, Aggarwal H, Tsai M-F, Soorian SS, Siliveri S, Goskula S, Gujjula SR, Narayanan V (2021) Rapid synthesis of a novel nano-crystalline mesoporous faujasite type metal-organic framework, ZIF-8 catalyst, its detailed characterization, and NaBH₄ assisted, enhanced catalytic Rhodamine B degradation. *Mater Today Commun* 26:101993. <https://doi.org/10.1016/j.mtcomm.2020.101993>
- Das TK, Ganguly S, Bhawal P, Remanan S, Mondal S, Das NC (2018) Mussel inspired green synthesis of silver nanoparticles-decorated halloysite nanotube using dopamine: characterization and evaluation of its catalytic activity. *Appl Nanosci* 8:173–186. <https://doi.org/10.1007/s13204-018-0658-3>
- Deng H, He H, Sun S, Zhu X, Zhou D, Han F, Huang B, Pan X (2019) Photocatalytic degradation of dye by Ag/TiO₂ nanoparticles prepared with different sol-gel crystallization in the presence of effluent organic matter. *Environ Sci Pollut Res* 26:35900–35912. <https://doi.org/10.1007/s11356-019-06728-0>
- Dyab AK, Abdallah EM, Ahmed SA, Rabee MM (2016) Fabrication and characterisation of novel natural *Lycopodium clavatum* sporopollenin microcapsules loaded in-situ with nano-magnetic humic acid-metal complexes. *J Encapsulation Adsorpt Sci* 6:109
- Ecer Ü, Şahan T, Zengin A (2021a) Synthesis and characterization of an efficient catalyst based on MoS₂ decorated magnetic pumice: an experimental design study for methyl orange degradation. *J Environ Chem Eng* 9:105265. <https://doi.org/10.1016/j.jece.2021.105265>
- Ecer Ü, Zengin A, Şahan T (2021b) Magnetic clay/zeolitic imidazole framework nanocomposite (ZIF-8@Fe₃O₄@BNT) for reactive orange 16 removal from liquid media. *Colloid Surf A* 630:127558. <https://doi.org/10.1016/j.colsurfa.2021.127558>
- Gola D, Kriti A, Bhatt N, Bajpai M, Singh A, Arya A, Chauhan N, Srivastava SK, Tyagi PK, Agrawal Y (2021) Silver nanoparticles for enhanced dye degradation. *Curr Res Green Sustain Chem* 4:100132. <https://doi.org/10.1016/j.crgsc.2021.100132>
- Gubbuk IH (2011) Isotherms and thermodynamics for the sorption of heavy metal ions onto functionalized sporopollenin. *J Hazard Mater* 186:416–422. <https://doi.org/10.1016/j.jhazmat.2010.11.010>
- Hassan AM, Wan Ibrahim WA, Bakar MB, Sanagi MM, Sutirman ZA, Nodeh HR, Mokhter MA (2020) New effective 3-aminopropyltrimethoxysilane functionalized magnetic sporopollenin-based silica coated graphene oxide adsorbent for removal of Pb(II) from aqueous environment. *J Environ Manage* 253:109658. <https://doi.org/10.1016/j.jenvman.2019.109658>
- He K, Yan M, Huang Z, Zeng G, Chen A, Huang T, Li H, Ren X, Chen G (2019) Fabrication of polydopamine-kaolin supported Ag nanoparticles as effective catalyst for rapid dye decoloration.

- Chemosphere 219:400–408. <https://doi.org/10.1016/j.chemosphere.2018.12.012>
- Ismail M, Khan MI, Khan SB, Khan MA, Akhtar K, Asiri AM (2018) Green synthesis of plant supported CuAg and CuNi bimetallic nanoparticles in the reduction of nitrophenols and organic dyes for water treatment. *J Mol Liq* 260:78–91. <https://doi.org/10.1016/j.molliq.2018.03.058>
- Jeyapragasam T, Kannan RS (2016) Microwave assisted green synthesis of silver nanorods as catalysts for rhodamine B degradation. *Russ J Phys Chem* 90:1334–1337. <https://doi.org/10.1134/S003602441607030X>
- Jyoti K, Baunthiyal M, Singh A (2016) Characterization of silver nanoparticles synthesized using *Urtica dioica* Linn. leaves and their synergistic effects with antibiotics. *J Radiat Res Appl Sci* 9:217–227. <https://doi.org/10.1016/j.jrras.2015.10.002>
- Khan ZUH, Shah NS, Iqbal J, Khan AU, Imran M, Alshehri SM, Muhammad N, Sayed M, Ahmad N, Kousar A, Ashfaq M, Howari F, Tahir K (2020) Biomedical and photocatalytic applications of biosynthesized silver nanoparticles: ecotoxicology study of brilliant green dye and its mechanistic degradation pathways. *J Mol Liq* 319:114114. <https://doi.org/10.1016/j.molliq.2020.114114>
- Kim MR, Lee DK, Jang D-J (2011) Facile fabrication of hollow Pt/Ag nanocomposites having enhanced catalytic properties. *Appl Catal B* 103:253–260. <https://doi.org/10.1016/j.apcatb.2011.01.036>
- Kohri M, Kohma H, Shinoda Y, Yamauchi M, Yagai S, Kojima T, Taniguchi T, Kishikawa K (2013) A colorless functional polydopamine thin layer as a basis for polymer capsules. *Polym Chem* 4:2696–2702. <https://doi.org/10.1039/C3PY00181D>
- Kong H, Jang J (2008) Synthesis and antimicrobial properties of novel silver/polyrhodanine nanofibers. *Biomacromol* 9:2677–2681. <https://doi.org/10.1021/bm800574x>
- Kumar A, Mishra B, Tripathi BP (2020) Polydopamine assisted synthesis of ultrafine silver nanoparticles for heterogeneous catalysis and water remediation. *Nano-Struct Nano-Objects* 23:100489. <https://doi.org/10.1016/j.nanoso.2020.100489>
- Kurtan U, Amir M, Yıldız A, Baykal A (2016) Synthesis of magnetically recyclable $\text{MnFe}_2\text{O}_4@ \text{SiO}_2@ \text{Ag}$ nanocatalyst: its high catalytic performances for azo dyes and nitro compounds reduction. *Appl Surf Sci* 376:16–25
- Li G, Li Y, Wang Z, Liu H (2017) Green synthesis of palladium nanoparticles with carboxymethyl cellulose for degradation of azo-dyes. *Mater Chem Phys* 187:133–140
- Li Y, Lu H, Wang Y, Li X (2019) Deposition of Au nanoparticles on PDA-functionalized PVA beads as a recyclable catalyst for degradation of organic pollutants with NaBH_4 in aqueous solution. *J Alloys Compd* 793:115–126. <https://doi.org/10.1016/j.jallcom.2019.04.148>
- Li Y, Wang Y, Lu H, Li X (2020a) Preparation of $\text{CoFe}_2\text{O}_4\text{-P}_4\text{VP}@ \text{Ag}$ NPs as effective and recyclable catalysts for the degradation of organic pollutants with NaBH_4 in water. *Int J Hydrog Energy* 45:16080–16093. <https://doi.org/10.1016/j.ijhydene.2020.04.002>
- Li Z, Yuan C-G, Guo Q, Wei X (2020b) Preparation of stable AgNPs@ PAN/GO-SH nanocomposite by electrospinning for effective degradation of 4-nitrophenol, methylene blue and Rhodamine B. *Mater Chem* 265:127409. <https://doi.org/10.1016/j.matlet.2020.127409>
- Lu Z, Xiao J, Wang Y, Meng M (2015) In situ synthesis of silver nanoparticles uniformly distributed on polydopamine-coated silk fibers for antibacterial application. *J Colloid Interface Sci* 452:8–14. <https://doi.org/10.1016/j.jcis.2015.04.015>
- Mishra K, Poudel TN, Basavegowda N, Lee YR (2016) Enhanced catalytic performance of magnetic $\text{Fe}_3\text{O}_4\text{-MnO}_2$ nanocomposites for the decolorization of rhodamine B, reduction of 4-nitroaniline, and sp3 C-H functionalization of 2-methylpyridines to isatins. *J Catal* 344:273–285. <https://doi.org/10.1016/j.jcat.2016.09.020>
- Mondal A, Adhikary B, Mukherjee D (2015) Room-temperature synthesis of air stable cobalt nanoparticles and their use as catalyst for methyl orange dye degradation. *Colloid Surf A* 482:248–257
- Nalbandian L, Patrikiadou E, Zaspalis V, Patrikidou A, Hatzidaki E, Papandreou N, C, (2016) Magnetic nanoparticles in medical diagnostic applications: synthesis, characterization and proteins conjugation. *Curr Nanosci* 12:455–468
- Naseem K, Begum R, Wu W, Irfan A, Al-Sehemi AG, Farooqi ZH (2019) Catalytic reduction of toxic dyes in the presence of silver nanoparticles impregnated core-shell composite microgels. *J Clean Prod* 211:855–864. <https://doi.org/10.1016/j.jclepro.2018.11.164>
- Şahan T, Öztürk D (2014) Investigation of Pb(II) adsorption onto pumice samples: application of optimization method based on fractional factorial design and response surface methodology. *Clean Technol Envir* 16:819–831. <https://doi.org/10.1007/s10098-013-0673-8>
- Salama A, Mohamed A, Aboamera NM, Osman TA, Khattab A (2018) Photocatalytic degradation of organic dyes using composite nanofibers under UV irradiation. *Appl Nanosci* 8:155–161. <https://doi.org/10.1007/s13204-018-0660-9>
- Sen TK, Afroze S, Ang HM (2011) Equilibrium, kinetics and mechanism of removal of methylene blue from aqueous solution by adsorption onto pine cone biomass of *Pinus radiata*. *Water Air Soil Pollut* 218:499–515. <https://doi.org/10.1007/s11270-010-0663-y>
- Su S, Guo W, Leng Y, Yi C, Ma Z (2013) Heterogeneous activation of oxone by $\text{Co}_x\text{Fe}_{3-x}\text{O}_4$ nanocatalysts for degradation of rhodamine B. *J Hazard Mater* 244–245:736–742. <https://doi.org/10.1016/j.jhazmat.2012.11.005>
- Touqeer T, Mumtaz MW, Mukhtar H, Irfan A, Akram S, Shabbir A, Rashid U, Nehdi IA, Choong TSY (2020) $\text{Fe}_3\text{O}_4\text{-PDA}$ -lipase as surface functionalized nano biocatalyst for the production of biodiesel using waste cooking oil as feedstock: Characterization and process optimization. *Energies* 13:177
- Uzuriaga-Sánchez RJ, Khan S, Wong A, Picasso G, Pividori MI, Sotomayor MDPT (2016) Magnetically separable polymer (Mag-MIP) for selective analysis of biotin in food samples. *Food Chem* 190:460–467. <https://doi.org/10.1016/j.foodchem.2015.05.129>
- Vanaja M, Annadurai G (2013) *Coleus aromaticus* leaf extract mediated synthesis of silver nanoparticles and its bactericidal activity. *Appl Nanosci* 3:217–223. <https://doi.org/10.1007/s13204-012-0121-9>
- Veerakumar P, Chen S-M, Madhu R, Veeramani V, Hung C-T, Liu S-B (2015) Nickel nanoparticle-decorated porous carbons for highly active catalytic reduction of organic dyes and sensitive detection of Hg(II) ions. *ACS Appl Mater Interfaces* 7:24810–24821. <https://doi.org/10.1021/acsami.5b07900>
- Wang J, Zhang Q, Shao X, Ma J, Tian G (2018) Properties of magnetic carbon nanomaterials and application in removal organic dyes. *Chemosphere* 207:377–384. <https://doi.org/10.1016/j.chemosphere.2018.05.109>
- Yılmaz Ş, Zengin A, Ecer Ü, Şahan T (2019) Conversion from a natural mineral to a novel effective adsorbent: utilization of pumice grafted with polymer brush for methylene blue decolorization from aqueous environments. *Colloid Surf A* 583:123961. <https://doi.org/10.1016/j.colsurfa.2019.123961>
- Zhang Y, Zhu P, Chen L, Li G, Zhou F, Lu D, Sun R, Zhou F, Wong C-p (2014) Hierarchical architectures of monodisperse porous Cu microspheres: synthesis, growth mechanism, high-efficiency and recyclable catalytic performance. *J Mater Chem* 2:11966–11973. <https://doi.org/10.1039/C4TA01920B>